Capillary-force measurement on SiC surfaces

M. Sedighi,[1,2] V. B. Svetovoy,[3,4] and G. Palasantzas[1]
[1]*Zernike Institute for Advanced Materials, University of Groningen, Nijenborgh 4, 9747 AG Groningen, Netherlands*
[2]*Department of Mechanical Engineering, Shahrood University of Technology, Shahrood, Iran*
[3]*MESA+ Institute for Nanotechnology, University of Twente, P.O. Box 217, 7500 AE Enschede, Netherlands*
[4]*Yaroslavl Branch of the Institute of Physics and Technology, RAS, Yaroslavl 150007, Russia*
(Received 2 March 2016; revised manuscript received 10 May 2016; published 24 June 2016)

Capillary forces have been measured by atomic force microscopy in the sphere-plate geometry, in a controlled humidity environment, between smooth silicon carbide and borosilicate glass spheres. The force measurements were performed as a function of the rms surface roughness ∼4–14 nm mainly due to sphere morphology, the relative humidity (RH) ∼0%–40%, the applied load on the cantilever, and the contact time. The pull-off force was found to decrease by nearly two orders of magnitude with increasing rms roughness from 8 to 14 nm due to formation of a few capillary menisci for the roughest surfaces, while it remained unchanged for rms roughness <8 nm implying fully wetted surface features leading to a single meniscus. The latter reached a steady state in less than 5 s for the smoothest surfaces, as force measurements versus contact time indicated for increased RH∼40%. Finally, the pull-off force increases and reaches a maximum with applied load, which is associated with plastic deformation of surface asperities, and decreases at higher loads.

DOI: 10.1103/PhysRevE.93.062803

I. INTRODUCTION

Capillary forces [1] are essential surface interactions in the technology of micro- and nanoelectromechanical systems (MEMS and NEMS) since they can lead to irreversible adhesion between moving components [2]. In general, adhesive forces between surfaces have several contributions, such as electrostatic forces, van der Waals (vdW) forces, capillary forces, and forces arising from physicochemical processes between interacting surfaces. For hydrophilic interfaces under ambient conditions, the dominant force usually is the capillary force associated with the formation of liquid capillary bridges between two surfaces. Furthermore, with the advent of atomic force microscopy (AFM), force distance curves measured between surfaces and AFM probes enabled measurements of capillary adhesion forces with pN to nN sensitivity [1]. Under ambient conditions the capillary forces impose an important restriction on accurate measurements with AFM of fundamental dispersion forces such as vdW and Casimir forces at close separations of ∼10 nm using colloidal probes with radius ∼10–100 μm. These forces have the same origin as a consequence of quantum fluctuations of the electromagnetic field with the vdW force being the short-range limit (typically <10 nm), while the Casimir force acts at longer separations (>20 nm) where retardation is important [3]. In fact, relatively stiff cantilevers (with spring constants $k \sim 4\mathrm{N/m}$) for colloid probe AFM force measurements still require several microns retraction distance due to capillary stiction [4,5]. However, for softer cantilevers, which offer higher force sensitivity, capillary forces lead to jump to contact and prohibit continuous force measurements since the cantilever must be retracted over distances even exceeding the range of the AFM piezo tube (>20 μm) [6].

Surface roughening and/or reduction of the relative humidity can provide a remedy for reducing the capillary forces so that dispersion force measurements with softer cantilevers ($k \sim 1$–$2\,\mathrm{N/m}$) could become feasible [4–6]. From previous works [5] it was concluded that the scaling of the capillary force with the rms roughness of two surfaces depends on the wetting properties of the material. Moreover, the knowledge of capillary forces between material surfaces, possessing attributes such as high durability combined with high stiffness and low thermal expansion, is important for a multitude of applications ranging from optical bonding to macroassembly, and MEMS technologies. Silicon carbide (SiC) is a material that offers the previous special attributes, and it is currently utilized for precise instrumentation frames and mirrors. There is also a possibility to be used in macro- and nanoassembly technologies via direct (optical) bonding [7]. Moreover, for MEMS applications, e.g., in the automotive industry and space applications [8,9], MEM sensors are required to operate in harsh environments that can be a challenge for Si devices, whereas SiC is considered a substitute for Si due to its excellent properties. In fact the limitation to Si-based MEMS is highly apparent in applications involving high temperature environments where diamond, gallium nitride (GaN), and SiC are considered the leading candidates. SiC is also an excellent material for high frequency NEMS since the ratio of its Young's modulus E to mass density ρ (also known as acoustic velocity) is significantly higher than for other semiconducting materials commonly used for electromechanical devices [10–12]. The relatively low residual stress level in the layers, the high stiffness, and excellent etch-stop properties allow the fabrication of freestanding SiC microstructures using standard Si bulk micromachining techniques [8,9]. Silicon carbide is also well suited as a protective coating of micromachined parts since it exhibits high hardness, chemical inertness, and ability to survive operation at high temperatures, as well as harsh corrosive environments [13,14]. Finally, SiC is one of the few semiconducting materials that combines biocompatibility and high sensing potential [12].

Since SiC samples can be fabricated very flat with rms roughness amplitudes of the order of ∼1 nm or less they have been used for dispersive force measurements at short ranges with borosilicate spheres (∼10 nm) [6]. Note for comparison that when Casimir and any remnant electrostatic

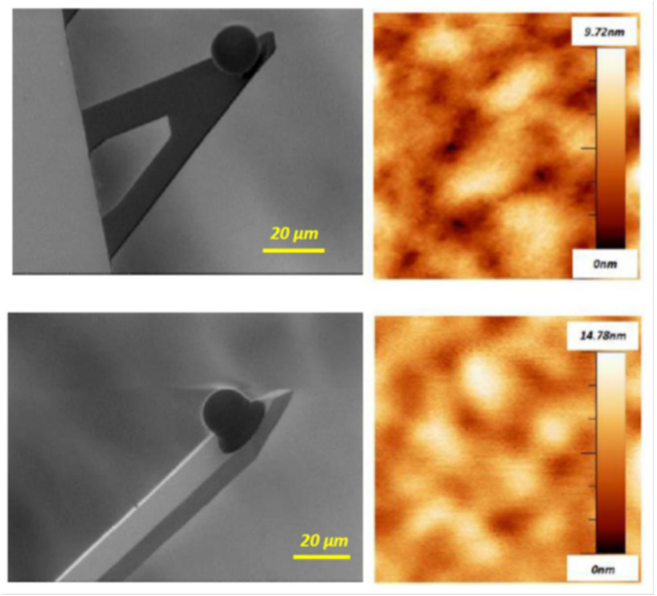

FIG. 1. AFM topography and height distribution of the borosilicate spheres roughness obtained by scanning ($800 \times 800\,\mathrm{nm}^2$ scan size) on top of the sphere (right) and top view scanning electron microscopy (SEM) image of a sphere attached on a cantilever (left).

forces cause cantilever bending up to ∼10 nm, the capillary forces easily account for bending in ambient of ∼600 nm or more. Therefore, here we study the capillary forces using the colloid probe AFM technique (Fig. 1). They will be measured versus surface roughness of the spherical probe and sample surface, relative humidity, applied load, and contact time of the probe onto the SiC surface. From the set of surface roughness parameters, our focus will be on the rms roughness amplitude since it has the major contribution on capillary forces as was shown in former experiments between rougher Au-Au surfaces [5].

II. EXPERIMENTAL PROCEDURE

For the force measurements nitrogen (N) doped SiC samples (thickness 400 μm and chemical-mechanical polished) were obtained from University Wafers [15]. For the measurement we used a Bruker Pico Force AFM operated in air as well as within a bell jar to achieve controlled humidity conditions. The bell jar, with the AFM embedded, could be evacuated down to $\sim 10^{-5}$ mbar and then refilled with any desired gas. The humidity was measured using a sensor (SHT75) with accuracy ∼1.8% and ∼2%–4% for relative humidity (RH) in the range RH∼10%–90% and for RH∼0%–10%, respectively, at room temperature (RT). In any case, before starting force measurements the RH was allowed to reach its equilibrium value by waiting for a half hour.

The force measurements were performed in the sphere-plate geometry where a 20-μm-diameter borosilicate sphere (Duke Scientific) was glued on Au coated tipless cantilevers (Fig. 1). We used a variety of cantilevers with spring constants $k = 2, 3, 5\,\mathrm{N/m}$. One relatively fast method to obtain the spring constant with accuracy ∼8%–10%, as we routinely performed for our cantilevers, is thermal tuning [16], which involves

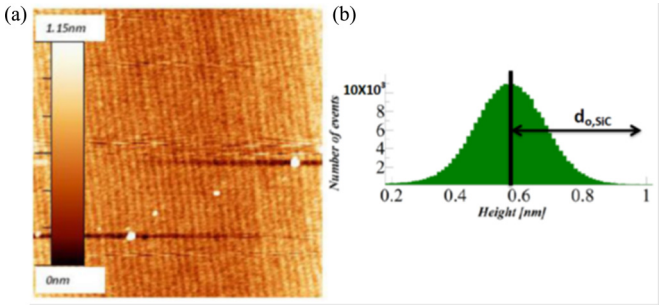

FIG. 2. (a) AFM topography and height distribution of the SiC sample ($4 \times 4\,\mu\mathrm{m}^2$ scan size). (b) Height distribution and distance upon conduct $d_{\mathrm{o,\,SiC}}$ due to SiC surface.

measuring the mechanical response of the cantilever due to agitations by impinging molecules from the surrounding fluid (e.g., air, gases, or liquids) and due to thermal dissipation via internal degrees of freedom. The thermal tuning method gave $k = 2 \pm 0.3\,\mathrm{N/m}$. For the used cantilevers more precise values based on the electrostatic calibration were available from earlier Casimir force measurements $k = 2 \pm 0.08\,\mathrm{N/m}$ [6], $k = 3 \pm 0.24\,\mathrm{N/m}$, $k = 5 \pm 0.38\,\mathrm{N/m}$.

During force measurement the piezo speed was 100 nm/s (the same for approach and retraction), while during studies of the effect of contact time on the capillary pull-off force the piezo speed changed between 100 nm/s and 5 μm/s. For each force measurement we obtained 27 force versus distance curves (40 000 points per curve) at three different points on the sample and finally the data were averaged to obtain the pull-off force. No significant variation was observed in the force data above the reported error bars. This is also expected because the SiC surfaces are very smooth. Finally, the topography of both the borosilicate sphere (Fig. 1) and the SiC plate (Fig. 2), which were used for the capillary-force measurements (Fig. 3), was inspected by AFM and by scanning electron microscopy (SEM) (see Fig. 1) after complete preparation and prior to

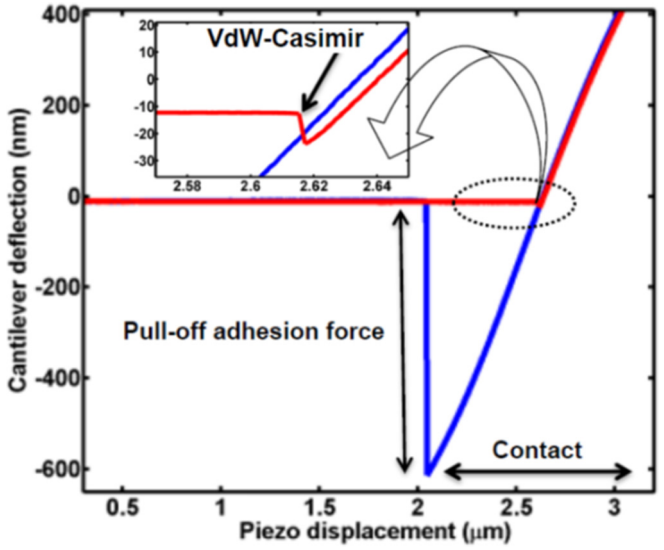

FIG. 3. Schematic representation of a force-distance curve. Red line represents approach and blue line retraction.

the force measurements. The rms roughness amplitude of SiC samples is shown in Fig. 2 with the corresponding height histogram indicating the contribution of the SiC surface in the distance upon contact $d_{o,SiC}$ between the interacting surfaces [17]. Note that the spheres with radius $R\sim10$ μm (or smaller) are rather restrictive for morphology measurements with an AFM due to curvature effects limiting the scan size to ~1 μm or less.

III. ANALYSIS OF THE FORCE MEASUREMENTS

Adhesion force measurements between Au-Au surfaces in the past indicated no significant influence of the RH on the measured forces in the range RH$\sim$15%–60% [5]. Here we performed similar measurements for humidity 2%$\leqslant$RH$\leqslant$40% indicating that for SiC surfaces, which are significantly smoother than evaporated Au surfaces, RH can play a significant role depending on surface roughness. The roughness analysis indicated almost atomically flat SiC surfaces with a root-mean-square (rms) surface roughness $w_{SiC} \approx 0.12$ nm [6,14]. Therefore, the maximum surface peak on SiC is at most $d_{o,SiC} \approx 0.5$–0.6 nm as obtained by the height histograms [6,18]. AFM measurement of the sphere roughness gave a maximum surface peak in the range $d_{o,sph} \approx 4$–40 nm ($d_{o,sph} \approx 4.5 w_{sph}$ where w_{sph} is the rms sphere roughness over an 800×800 nm^2 scan area, while in all cases we have $w_{SiC} \ll w_{sph}$). Therefore, the maximum total distance upon contact of the sphere on the SiC surface limited due to random surface roughness (of both interacting surfaces) is estimated to be $d_{o,max} \approx d_{o,SiC} + d_{o,sph}$ if the highest peak at the SiC surface and the sphere surface are at the same location [17]. The latter is rarely true and for an average estimate for d_o (with $d_o < d_{o,max}$) we consider $d_o \approx w_{SiC} + d_{o,sph} (\geqslant 4$ nm) since the SiC sample is smooth and the main roughness contribution comes from the sphere surface features [6]. Note that the AFM scan sizes are larger than the typical interaction area $A_{int} \approx \pi d_o R$ for a colloid probe of radius R [17], and it makes it possible to capture the necessary roughness wavelengths of both interacting surfaces. In any case these values of d_o indicate that the sphere can still approach the plate at a separation less than 10 nm, which is limited only due to jump to contact by formation of a large capillary meniscus.

Spontaneous vapor condensation and formation of a capillary meniscus (both interacting surfaces are hydrophilic) will lead to jump to contact at separations $>d_o$. The latter occurs when the surface separation is comparable to $\approx 2R_k$, where $R_k = -(\gamma V_m/\mathrm{RT})[\log(\mathrm{RH})]^{-1}$ with γ being the liquid surface tension and V_m the molar liquid volume [1,19]. For water at $T = 300$ K and $\gamma = 73$ mJ/m^2 ($\gamma V_m/\mathrm{RT} = 0.54$ nm [17]) we obtain $2R_k \approx 0.5-2.7$ nm for RH$\approx$1%–40% [16]. Therefore, the minimum possible separation prior to jump to contact is estimated to be $d_{min} \approx d_o + 2R_k$, where substitution yields $d_{min} > 5$ nm for the smoothest surfaces. Note that even when the AFM was pumped at a pressure as low as $\sim10^{-5}$ mbar and vented several times with dry N_2, the water surface layer on hydrophilic surfaces, and the associated capillary forces, can only be reduced but not fully eliminated [1,5,19–22].

It is important to estimate the upper and lower limits for the pull-off adhesion force in the case of strong and weak surface roughness, respectively. For the relatively smooth surfaces the pull-off capillary force is defined by a large meniscus, and

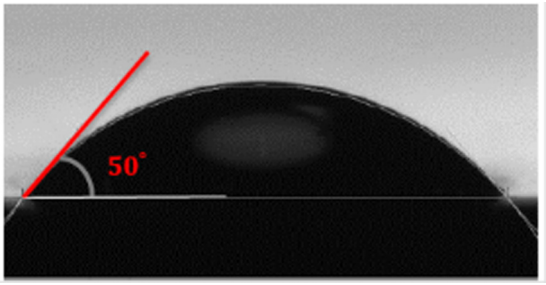

FIG. 4. Contact angle measurement of a water droplet on the SiC surface.

ignoring weak vdW interaction one has [21]

$$F_c = 2\pi\gamma R[\cos(\theta_1) + \cos(\theta_2)], \quad (1)$$

where θ_1 and θ_2 are the contact angles on the plate and the sphere, respectively, and R is the sphere radius. The angles are estimated as $\theta_{1(SiC)} = 50^\circ$ [21] and $\theta_{2(borosilicate)} = 30^\circ$ [5]. We also measured the contact angle on SiC to be $50^\circ\pm5^\circ$ (see Fig. 4). Therefore, the force between smooth sphere and plate surfaces with one large meniscus coincides with the upper force limit that yields $F_{c,u}/R = 2\pi\gamma\sum_{i=1}^{2}\cos(\theta_i)$ (Fig. 6). For rough surfaces, where contact down to a single or few asperities is possible [with formation of nanosize capillary bridges, Fig. 5(b)], R represents an average asperity radius $R_{asp} \approx 135$ nm. Since the SiC surface is much smoother than that of the sphere, $w_{SiC} \ll w_{sph}$, the top of an asperity can be well approximated by a sphere. Therefore the average asperity radius R_{asp} was derived from the size of asperities of rough spheres with rms $>$ 14nm), and yields a lower force limit $F_{c,l}/R = 2\pi\gamma(R_{asp}/R)\sum_{i=1}^{2}\cos(\theta_i)$ (Fig. 6).

Figure 6 shows the adhesion pull-off force measured as a function of roughness of both the sphere and the sample. With increasing rms surface roughness up to 8 nm no significant change of the pull-off force is observed (beyond the error bars)

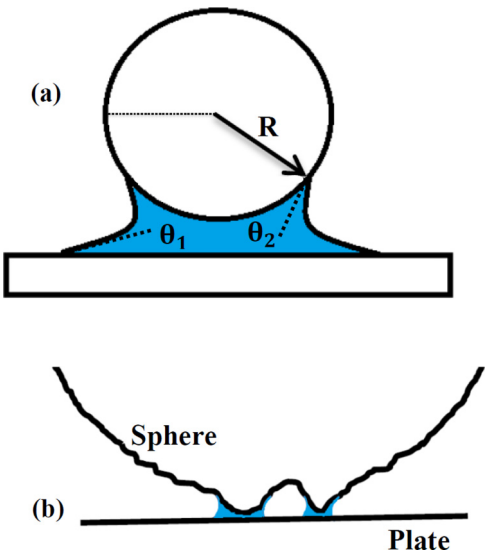

FIG. 5. (a) Schematic of water meniscus between a sphere and a plate. (b) Schematic of capillary condensation between rough surfaces, where menisci form at contact of asperities.

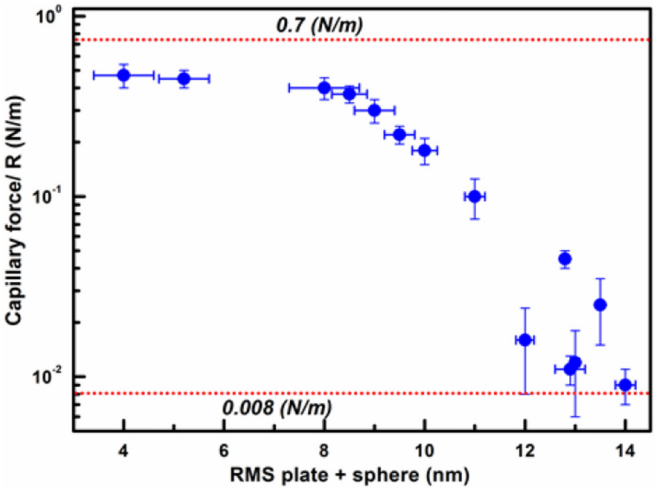

FIG. 6. Force measurements versus rms surface roughness of both sphere and sample (in air) using spheres with varying roughness as the AFM inspection also indicated. The theory prediction via Eq. (1) for the upper (using the sphere tip radius $R = 10\,\mu$m) and lower (using an asperity radius $R_{\rm sph} \approx 135$ nm) force limits (horizontal lines).

indicating that the capillary meniscus is formed over a large area upon sphere-sample contact. The measured force values are close to the upper limit predicted by Eq. (1). However, for rms roughness above 8 nm the pull-off capillary force drops drastically. For an additional increment of 6 nm in the rms roughness the force decreases by nearly two orders of magnitude. The lowest force values are close to the theory prediction, $F_{c,l}/R$, where only a few menisci form capillary bridges.

The measured capillary pull-off forces can also be related to the capillary bridge height (BH) between the rough contacting surfaces [5]. Indeed, the water bridge that wets both the sphere and the sample surfaces must be higher than the roughness peak upon contact $d_{\rm o}(\approx w_{\rm SiC} + d_{\rm o,sph})$. If the water bridge is smaller than $d_{\rm o}$ then the force drops rapidly (Fig. 6). For SiC the pull-off force drops by an order of magnitude of the maximum measured force while the rms roughness increases from 8 to 12 nm. For the rms ~ 8 nm the corresponding distance upon contact is $d_{\rm o} \approx 40$ nm ($d_{\rm o} \approx 4.5 \times$ rms [17]) and therefore BH ≈ 40 nm ($\gg 2R_k$). As a result the water layer thickness (d_w) that contributes each of the smoother surfaces on the meniscus is approximately $d_w \sim 20$ nm yielding a pull-off force close to the upper force limit (Fig. 6). If $d_{\rm o,1/10}$ is the distance upon contact due to roughness, where the adhesive force drops by an order of magnitude, then since $d_{\rm o,1/10} \approx 4.5 \times$ rms [17] and with rms $\approx$ 12 nm we obtain $d_{\rm o,1/10} \approx 54$ nm. In this case the water layer BH is significantly smaller than $d_{\rm o,1/10}$ with only a few asperities forming capillary meniscus around their apex [Fig. 5(b)] so that BH $\leqslant d_{\rm o,\,1/10}$–$2d_w$ or in the present case BH$\leqslant$14 nm.

Moreover, the formation of the capillary bridge is a dynamic process that depends on the contact time [23] that is measured by the point of contact during approach and retraction as shown in Fig. 3. If we denote with V_p the AFM piezo speed (the same for approach and retraction) then if $d_{\rm ap\text{-}ret}$ is the distance the

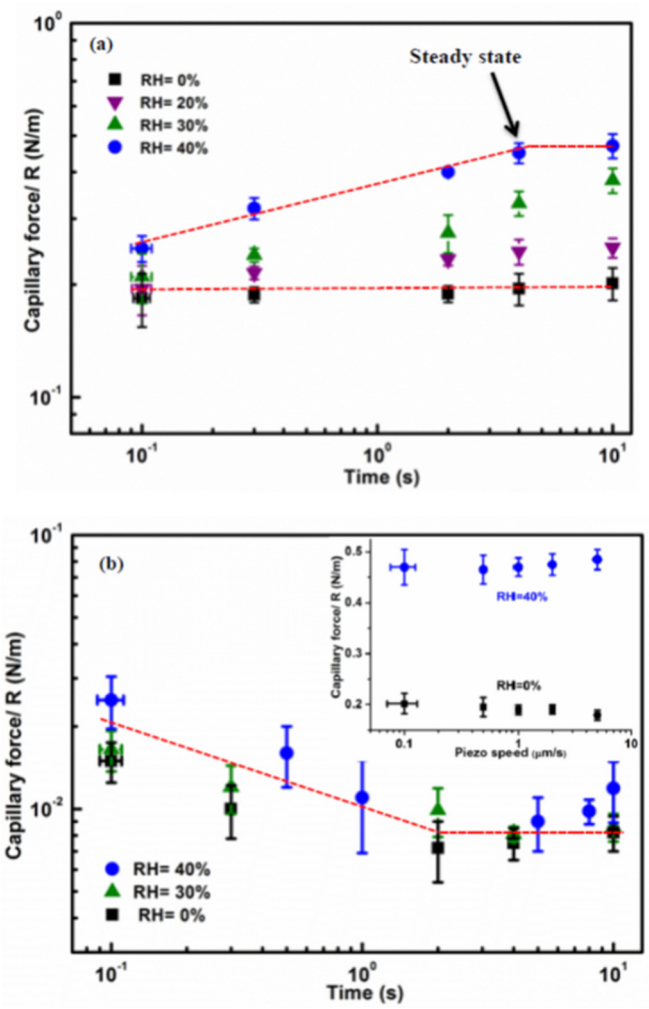

FIG. 7. Adhesion force measured as a function of the contact time at different relative humidity for (a) smoothest sphere, and (b) roughest sphere. The inset shows the capillary force versus piezo speed for two different values of RH as indicated.

piezo moves from the point of contact (during approach and retraction) and $d_{\rm adh}$ is the distance it moves from the point of contact before pull-off, then the total contact time is defined as $t \approx 2(d_{\rm ap\text{-}ret}/V_p) + (d_{\rm adh}/V_p)$. The latter can be controlled by altering the approach or retraction piezo speed, the piezo ramp size, and the applied load on the sphere (Fig. 7). Butt *et al.* [24] extensively investigated the kinetics of capillary bridge formation. They pointed out that the meniscus is formed in less than 1 ms, which shows that the speed of the piezo can have an effect on the capillary force at very short time scale ($\sim$1 ms, while in our case we probe much longer time scales of $\geqslant$100 ms). Additionally, this factor might play a role in a single tip system [25]. In order to exclude any possible dependence of the adhesion in piezo retract speed in our experimental results, we illustrate in the inset of Fig. 7(b) that the capillary force has no dependence on the piezo speed within the error bar of the force measurement. Usually capillary bridges form and rupture quickly. The meniscus can break if the retraction velocity is high and the liquid is viscous, which also makes the meniscus kinetically unstable [26,27]. For multiple asperities (as is case

for the sphere-plate setup) with no direct contact, the formation of a capillary bridge is an activated process. This could strongly influence the time dependence of the capillary force [23,24]. However, in our experiment the minimum contact time was 100 ms (Fig. 7), which is much larger than the time where the speed of the piezo could play any significant role.

Figure 7(a) shows that the pull-off capillary force for the smoothest sphere (Fig. 6, rms ~ 4 nm) remains unaffected by increasing the contact time at very low relative humidity (RH $\sim$ 0%) within the error bar of the force measurement. One can see from Fig. 7(a) that with increasing RH the force increases with contact time and reaches a steady state (saturation) at $\sim$5 s for RH = 40%, while for lower RH the force is still increasing with increases of contact time. An approximate linear fit gave an increment with the contact time t : $\ln[F/R]_{\mathrm{RH}=40\%} = 3.5 \times 10^{-2} t + 0.32$, and $\ln[F/R]_{\mathrm{RH}=30\%} = 2.9 \times 10^{-2} t + 0.22$ for different RH indicating the steeper increase of the pull-off force with contact time to reach saturation faster at higher RH.

On the other hand, for the roughest sphere (Fig. 6, rms $\sim$ 14 nm), which is close to the lowest pull-off force limit, the force increases with increasing humidity but as a functions of the contact time it decreases, reaching steady state at $t \sim 2$ s. It is apparently the time for stabilization of the capillary bridge, which further remains unaffected within the error bars. These findings are in agreement with the previous studies of the contact time between Au-Au surfaces. The latter, however, were performed for significantly higher RH ($\sim$60%) [5], while here we investigated different values of RH. The stabilization times for the smoother Au-Au surfaces (total rms roughness 3.5 nm) were significantly longer ($\geqslant$100 s) [5]. These differences show that the morphology details here and in [5], besides the rms roughness, can have also significant impact on the temporal evolution of capillary bridges.

Measurements of the pull-off capillary force as a function of applied load indicated similar behavior for the smoothest and roughest spheres at different RH, but the magnitude of the changes depended on roughness (Fig. 8). The maximum capillary force is observed at the same applied load, which could indicate that at this load significant plastic deformation of the asperities sets in. In fact, the compressive stresses of the involved materials are $\sim$2 and $\sim$1.38 GPa for borosilicate glass and SiC, respectively [28]. For a sphere with $R = 10\,\mu$m, the contact pressure at the effective interaction area between the sphere and the plate ($\sim \pi d_o R$) reaches a value of $\sim$1.5 GPa, which is comparable to the compressive strength of both borosilicate glass and SiC. Therefore, we cannot neglect plastic deformations when the bodies come into contact for the applied loads, which can be very significant, especially for the sharp asperities [5]. As a result borosilicate spheres which have a major contribution to the total roughness will experience plastic deformation. For instance, for asperities with radius $R_{\mathrm{asp}} \approx 120$ nm the contact pressure is $\sim$76 GPa, which is significantly higher than the corresponding compressive stresses, and thus sufficient to cause plastic deformation of asperities on the sphere surface.

In both cases, for the smoothest and roughest spheres, the force increased with humidity and reached a maximum with increasing applied load indicating that plastic deformation of surface features takes place. The latter has more prominent

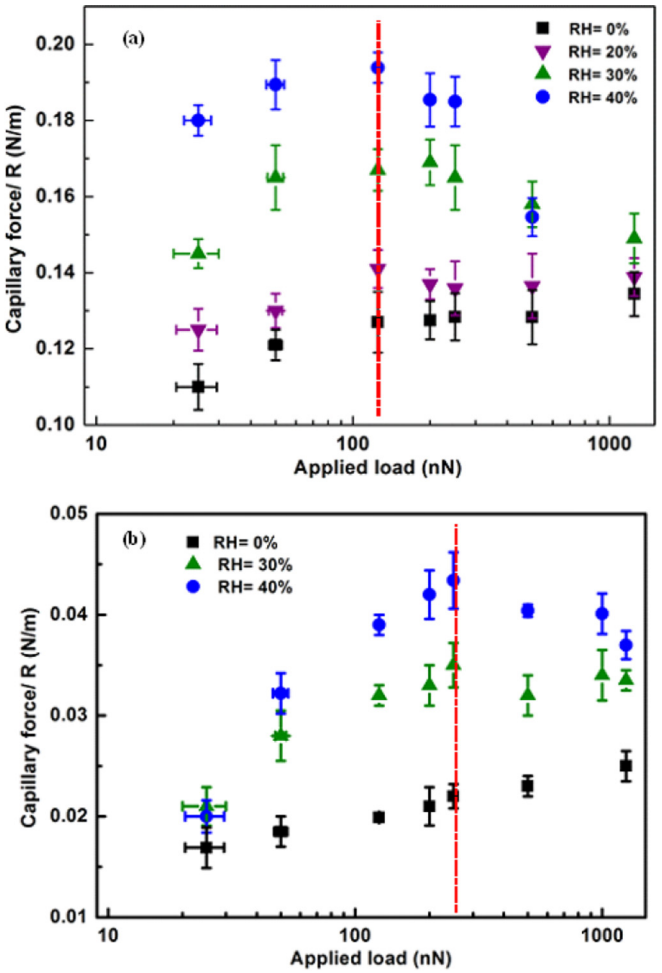

FIG. 8. Adhesion force measurements as a function of applied load (with the maximum indicated) at different relative humidities for (a) smoothest sphere, and (b) roughest sphere.

effect for the smoother surfaces. This is likely to happen because for rougher surfaces only a few asperities participate in menisci formation. However, for RH $\sim$ 0% the force in both cases was basically increased with increasing load indicating the capillary bridge(s) were still evolving due to limited water layer thickness on the interacting surfaces. Moreover, if we compare the maximum position, then for the smoothest surface it occurs for applied load $F_{\mathrm{ap}} \sim 140$ nN, while for the roughest case it takes place for an almost double force load $F_{\mathrm{ap}} \sim 260$ nN since in this case the surface features are larger and therefore require higher load to plastically deform. Notably with increasing humidity the maximum took place at the same applied load as long as RH>20%.

IV. CONCLUSIONS

Capillary forces have been measured by atomic force microscopy in the sphere-plate geometry, within a controlled humidity environment, between relatively smooth silicon carbide (plane) and borosilicate glass (sphere) surfaces. The pull-off capillary force was found to decrease by nearly two orders of magnitude when rms roughness increases from 8 to 14 nm due to formation of a few capillary menisci for

the roughest surfaces, while it remained unchanged for rms roughness <8 nm implying the formation of wetted surface features leading to a single meniscus. The latter reached a steady state in less than 5 s for the smoothest surfaces as pull-off force measurements versus contact time indicated (for RH $\sim 40\%$). Finally, the capillary pull-off force increases with humidity and reaches a maximum with applied load, while at even higher loads it decreases. The maximum is associated with plastic deformation of surface asperities since it takes place for similar loads under different humidity conditions. In future studies the dynamics of the capillary water bridges versus morphology will be further explored at different relative humidity and applied force load.

ACKNOWLEDGMENT

We would like to acknowledge support from the Zernike Institute of Advanced Materials, University of Groningen, Netherlands.

[1] H. J. Butt, B. Cappella, and M. Kappl, Surf. Sci. Rep. **59**, 1 (2005); J. Israelachvili, *Intermolecular and Surface Forces*, 3rd ed. (Elsevier Science Publishing, Amsterdam, 2011); A. W. Adamson and A. P. Gast, *Physical Chemistry of Surfaces* (Wiley, New York, 1997); R. Maboudian and R. T. Howe, J. Vac. Sci. Technol. B **15**, 1 (1997).

[2] K. L. Ekinci and M. L. Roukes, Rev. Sci. Instrum. **76**, 061101 (2005); A. Cleland, *Foundations of Nanomechanics* (Springer, New York, 2003).

[3] A. W. Rodriguez, F. Capasso, and S. G. Johnson, Nat. Photonics **5**, 211 (2011); P. Ball, Nature (London) **447**, 772 (2007); H. B. G. Casimir, Proc. K. Ned. Akad. Wet. **51**, 793 (1948); E. M. Lifshitz, Sov. Phys. JETP **2**, 73 (1956).

[4] P. J. van Zwol, G. Palasantzas, and J. T. M. De Hosson, Phys. Rev. B. **77**, 075412 (2008); Appl. Phys. Lett. **92**, 054101 (2008).

[5] P. J. van Zwol, G. Palasantzas, and J. Th. M. De Hosson, Phys. Rev. E **78**, 031606 (2008); Appl. Phys. Lett. **91**, 101905 (2007).

[6] M. Sedighi, V. B. Svetovoy, and G. Palasantzas, Phys. Rev. B **93**, 085434 (2016).

[7] J. Haisma, N. Hattu, J. T. C. M. Pulles, E. Steding, and J. C. G. Vervest, Appl. Opt. **46**, 6793 (2007); J. Haisma and G. A. C. M. Spierings, Philips J. Res. **49**, 47 (1995); Mater. Sci. Eng. R, **37**, 1 (2002).

[8] R. Cheung, Introduction to silicon carbide (SiC) microelectromechanical systems (MEMS), in *Silicon Carbide Microelectromechanical Systems for Harsh Environments*, edited by R. Cheung (University of Edinburgh, UK, 2006), Chap. 1.

[9] B. Stark, *MEMS Reliability Assurance Guidelines for Space Applications*, Jet Propulsion Laboratory Publication No. 99-1 (1999).

[10] C. A. Zorman and R. J. Parro, Phys. Status Solidi B **245**, 1404 (2008).

[11] A. D. Kurtz, T. A. Nunn, and R. A. Weber, US Patent No. 4,672,354 (1987).

[12] A. Lloyd Spetz and S. Savage, in *Silicon Carbide—Recent Major Advances*, edited by W. J. Choyke, H. Matsunami, and G. Pensl (Springer-Verlag, Berlin, Heidelberg, 2003), p. 869; X. Li, X. Wang, R. Bondokov, J. Morris, Y. H. An, and T. S. Sudarshan, J. Biomed. Mater. Res. Part B **72B**, 353 (2005).

[13] MRS Bull., Silicon Carbide Electronic Materials and Devices, **22**, 19 (1997).

[14] P. M. Sarro, Sens. Actuators, A **82**, 210 (2000).

[15] http://www.universitywafer.com/.

[16] B. Ohler, Rev. Sci. Instrum. **78**, 063701 (2007).

[17] P. J. van Zwol, V. B. Svetovoy, and G. Palasantzas, Phys. Rev. B **80**, 235401 (2009); V. B. Svetovoy and G. Palasantzas, Adv. Colloid Interface Sci. **216**, 1 (2015).

[18] M. Sedighi, V. B. Svetovoy, W. H. Broer, and G. Palasantzas, Phys. Rev. B **89**, 195440 (2014).

[19] H.-J. Butt, Langmuir **24**, 4715 (2008).

[20] F. W. Del Rio, M. L. Dunn, L. M. Phinney, C. J. Bourdon, and M. P. de Boer, Appl. Phys. Lett. **90**, 163104 (2007).

[21] A. de Lazzer, M. Dreyer, and H. J. Rath, Langmuir **15**, 4551 (1999); L. R. Fisher and J. N. Israelachvili, J. Colloid Interface Sci. **80**, 528 (1981); A. Ata, Y. I. Rabinovich, and R. K. Singh, J. Adhes. Sci. Technol. **16**, 337 (2002).

[22] L. Sirghi, R. Szoszkiewicz, and E. Riedo, Langmuir **22**, 1093 (2006).

[23] L. Bocquet, E. Charlaix, S. Ciliberto, and J. Crassous, Nature **396**, 735 (1998).

[24] H. J. Butt and M. Kappl, Adv. Colloid Interface Sci. **146**, 48 (2009).

[25] H. Gojzewski, M. Kappl, A. Ptak, and H.-J. Butt, Langmuir **26**, 1837 (2010); M. Farshchi-Tabrizi, M. Kappl, Y. J. Cheng, J. Gutmann, and H. J. Butt, *ibid.* **22**, 2171 (2006).

[26] S. Cai and B. Bhushan, Philos. Trans. R. Soc., A **366**, 1627 (2008).

[27] O. Pitois, P. Moucheront, and X. Chateau, J. Colloid Interface Sci. **231**, 26 (2000).

[28] For some indicative values of the compressive stress of SiC and borosilicate glass, respectively, see https://www.memsnet.org/material/siliconcarbidesicbulk/ and http://www.makeitfrom.com/material-properties/Borosilicate-Glass.